Materials Advances

PAPER

View Article Online
View Journal | View Issue

Cite this: *Mater. Adv.*, 2025, **6**, 1107

Logic-OR gate gold nanorod-based plasmonic biosensor for multipathogen detection and photothermal disinfection†

Francesca Petronella, *[a] Daniela De Biase, [b] Carlo Santini,[c] Arianna Avitabile,[b] Maria Laura Sforza, [b] Federica Zaccagnini, [b] Antonio d'Alessandro [c] and Luciano De Sio *[b]

Received 27th September 2024,
Accepted 2nd January 2025

DOI: 10.1039/d4ma00978a

rsc.li/materials-advances

Climate and demographic changes necessitate new paradigms to ensure equitable access to safe drinking water, limiting health, economic, and social damage from poor water management. Nanomaterials present promising opportunities in this area. This work addresses two relevant issues for safe water access: potable water monitoring and disinfection by leveraging plasmonic nanoparticles' biorecognition and photothermal properties. Colloidal gold nanorods (AuNRs), known for their sensitivity to local refractive index changes and light-to-heat conversion ability, are used to create AuNR arrays with optimal morphological and optical characteristics. We demonstrate that these biofunctionalized AuNR arrays, mimicking a logic-OR gate, can detect multiple bacterial strains in water, specifically recognizing two bacterial strains often monitored to guarantee safe access to potable water: *Escherichia coli* and *Salmonella typhimurium* (10^3 CFU per mL). The two strains are recognized separately or simultaneously, highlighting the multiplexing capability of the AuNR array. Furthermore, the exceptional light-to-heat conversion of AuNR arrays in a 'cascade-like' configuration, validated by a custom theoretical model, is utilized for photothermal disinfection. In a customized thermo-optical setup, this system effectively reduces pathogen viability by five orders of magnitude within 30 minutes under NIR laser irradiation. The bioactivated AuNR arrays, with their selective pathogen recognition and robust disinfection capabilities, represent a powerful multifunctional technology for monitoring and purifying potable water.

Introduction

Contamination of water with harmful pathogens presents serious health risks.[1] Pathogens such as bacteria, viruses, and parasites are responsible for waterborne diseases that affect human health and have significant economic consequences. Prompt and accurate identification of harmful pathogens is essential for timely intervention, preventing the spread of waterborne diseases. For this reason, ongoing research and innovation are needed to develop effective early-warning systems for water quality management and public health protection. Early warning systems are instrumental in safeguarding public health by detecting potential threats to water quality. Advanced detection and monitoring systems, including biosensors, are critical for ensuring water safety.[2] Biosensors are analytical devices that combine transducers with biological molecules and biochemical reactions to detect chemical or biological compounds through electrical, thermal, piezoelectric, or optical readouts.[3]

In cases of intentional or unintentional water contamination, point-of-use (POU) water disinfection is often regarded as the most practical solution for ensuring safe drinking water. Standard POU treatment technologies include chlorination, ozonation, water boiling, and solar disinfection (SODIS), divided into UV and photothermal (PT) disinfection.[4,5]

Chemical treatment methods require consumable materials and exhibit risks related to the growth of antibiotic-resistant pathogens and the formation of toxic disinfection by-products (DBPs). In addition, some of these techniques, such as chlorination, also produce undesirable odors or tastes.[6]

---

[a] *National Research Council of Italy, Institute of Crystallography CNR-IC, Montelibretti Division, Area territoriale di Ricerca di Roma 1, Strada Provinciale 35d, no. 9, 00010 Montelibretti, RM, Italy. E-mail: francesca.petronella@cnr.it*
[b] *Department of Medico-Surgical Sciences and Biotechnologies, Sapienza University of Rome, Corso della Repubblica 79, 04100 Latina, Italy. E-mail: luciano.desio@uniroma1.it*
[c] *Department of Information Engineering, Electronics and Telecommunications, Sapienza University of Rome, Via Eudossiana no. 18, 00184 Rome, Italy*

† Electronic supplementary information (ESI) available: Schematic representation of cascade AuNRs array; sensitivity to *n* change; statistical analysis on SEM micrographs; thermal response model of the microscopic system: methods (PDF). See DOI: https://doi.org/10.1039/d4ma00978a

Boiling water is the most recognized form of household water treatment to kill viruses, parasites, and bacteria without DBPs.[7,8] This method requires significant energy from burning chemical fuel or electrical heating, making it unsuitable for large-scale water disinfection. Solar energy for water disinfection is an attractive approach, as it uses a renewable, and therefore sustainable, source of energy. UV-based disinfection is very effective and extensively used for inactivating microorganisms.[8] Nevertheless, it requires artificial light sources as the atmosphere absorbs most UV radiation in the solar spectrum. In contrast, PT disinfection represents a promising avenue in antimicrobial technologies.[9–11] Indeed, this process leverages the distinctive properties of suitable light-harvesting materials to generate heat under light irradiation.[12] The application of PT disinfection strategies has expanded over the years, encompassing a wide range of materials as light-to-heat transducers.[12]

Plasmonic nanoparticles (NPs), including those based on noble metals like Au and Ag, represent a class of unique nanomaterials because they possess multifunctional properties. These NPs harness the localized surface plasmon resonance (LSPR) effect,[13] promoting a remarkable sensitivity to the change of the refractive index (n) of the surrounding medium. They also highly efficiently convert light into heat and generate hot carriers. These properties make NPs appealing for achieving innovative biosensors for water monitoring and PT disinfection. Noble metal NPs exhibit unique plasmonic properties that can be modulated by varying size and shape.[14] Accordingly, the absorption properties of noble metal NPs are tunable in the visible and near-infrared (NIR) wavelength range, which accounts for ~90% of the solar spectrum that reaches Earth. Remarkably, the morphological properties of plasmonic NPs significantly impact the n sensitivity and the efficacy of PT disinfection. Indeed, Loeb and co-workers investigated the PT disinfection capability of Au nanocubes (NCs) and nanorods (NRs). Their outcomes revealed a solid link between the morphology and the PT performance of Au NPs. In particular, they demonstrated superior PT disinfection properties for Au NRs.[15] In addition, it has been demonstrated that anisotropic Au nanostructures, including AuNRs, possess optimal optical performance for realizing highly sensitive plasmonic-based colorimetric biosensors.[16] However, to fully and simultaneously exploit the detection capability of Au NRs and their thermo-optical properties, preserving the optical features exhibited in the colloidal state while immobilizing them on a rigid platform is crucial. Nanofabrication techniques such as e-beam lithography are the best for exploiting this possibility. However, these processes are too expensive and allow only a reduced working area (a few mm^2)[17] to be fabricated. To overcome this issue, we have recently reported a novel technique that exploits a layer-by-layer electrostatic immersion process that allows the random organization on rigid substrates of AuNRs, resulting in AuNR arrays.[18] They exhibit, on a dry state, the colloidal dispersion's optical and thermo-optical properties. In addition, the technique allows an easy scaling up in terms of large-area fabrication and reproducibility. Moreover, using the same bottom-up technique to immobilize nanomaterials with different morphology, size, and composition on several substrates is possible.[17,19,20] Furthermore, the ability of the AuNR array was recently demonstrated to achieve PT disinfection of surfaces under NIR (resonant), and white light irradiation.[21] Compared to literature studies addressing similar issues,[22,23] this device mimics the functionality of an antibody-activated logic-OR gate. Remarkably, the biosensing performance leverages on the high n sensitivity of AuNRs with respect to Au NPs. As previously reported,[18,23,24] the proposed device offers additional advantages, such as an optical transducer immobilized on a substrate rather than dispersed in a liquid medium. Moreover, it relies on readily available instruments rather than requiring a complex facility, thus enhancing its practicality and accessibility.[18,25] Additionally, the bioactivation with a suitable recognition element, such as an antibody, has been effectively utilized to develop a versatile and reusable biosensor capable of detecting harmful bacteria in potable water.[17,26] Building on these promising results, we have developed an innovative multifunctional optical device designed to recognize multiple bacterial strains in potable water. This device mimics the functionality of an antibody-activated logic-OR gate. Furthermore, by harnessing the cascade-like geometry of the same AuNR array, we successfully demonstrated PT disinfection of tap water contaminated with harmful bacteria under NIR laser irradiation. Although, as already demonstrated,[21] the AuNR array works very well upon white light irradiation, we performed the experiments using a NIR source to validate the experimental results using a theoretical model while reducing the computational time. In particular, the present work points out the ability of the plasmonic cascade AuNR array to produce a PT heating that can disinfect the bulk volumes of tap water.

To respect our recent findings,[18,23] the present work highlights two significant advancements: first, our findings demonstrate that the proposed logic-OR gate plasmonic array can independently or simultaneously detect various bacterial strains, showcasing the device's multiplexing capability. The *E. coli* and *S. thyphimurium* selected for the present work are crucial in implementing POU water monitoring system. These bacteria are commonly monitored indicators of waterborne pathogens that pose significant risks to public health. Second, we established the multifunctionality of the platform by employing it for both pathogen detection and water disinfection in real time. Indeed, when configured in cascade platforms and activated by an NIR light source, the AuNR array induces a temperature increase sufficient for effective tap water disinfection. This evidence is the first demonstration of a disinfection process that extends beyond the device itself to the surrounding bulk water, thereby proving the transitiveness of the disinfection mechanism.

Through this experimental investigation, we set the basis to develop an innovative multifunctional device with the extraordinary capability to selectively recognize bacterial strains and to generate advanced and affordable PT disinfection strategies that can be harnessed for effective microbial control in diverse settings, especially in the disinfection of large volumes of water to make it potable, in particular in disadvantaged areas worldwide.

Experimental

Materials

Glass slides were purchased from Menzel Gläser. Citrate Capped Gold Nanorods (55 nm × 15 nm, AuNRs) were purchased from Nanocomposix, poly(sodium 4-styrenesulfonate) (PSS, M_w 70 000 Da), poly(allylamine hydrochloride) (PAH, M_w 50 000 Da), acetone, isopropanol, and methanol were purchased from Merck. Sodium chloride (NaCl) was purchased from Sigma-Aldrich, and NOA-61 was purchased from Norland. The anti-*Escherichia coli* antibody 1011 (AbE) was purchased from Santa Cruz Biotechnology, while the anti-*Salmonella typhymurium* antibody (ab8274, hereafter AbS) was purchased from Abcam. *Escherichia coli* (*E. coli*) K12 strain MG1655 (CGSC 7740) was obtained from the CGSC (Coli Genetic Stock Centre) collection. *Salmonella typhimurium* (*S. typhimurium*) LT2 was from ref. 27. Chemical minimal mediums for the growth of bacteria were purchased from Merck or VWR International. Components for LB medium were obtained from Life Technologies Italia.

AuNR array preparation

The AuNR arrays were fabricated by optimizing the protocol described in ref. 18. Glass substrates (1.5 cm × 1.5 cm or 1 cm × 1 cm) were cleaned by sequential sonication for 10 min in methanol and acetone baths, followed by an intermediate rinsing step in isopropanol, dried under nitrogen flow and modified with the polyelectrolytes multilayer (PEM) by assembling the sequence PAH/PSS/PAH.

The PEM was fabricated by sequential immersion of the glass substrate in PAH, PSS, and PAH solutions (1.6 mg mL^{-1}) for 10 min. An intermediate washing step in NaCl 0.5 M was performed between two consecutive PE solution immersions. Finally, the PEM-functionalized glass substrate was rinsed in water and dried under nitrogen flow. The incorporation of AuNRs was achieved by immersing the PEM-modified glass substrate in a water dispersion of AuNRs with an optical density of 1 (at 790 nm) for 20 h. After the immersion, the resulting AuNR array was washed with Milli-Q$^{®}$ water, dried with a nitrogen stream, and stored in the dark. A sketch of the AuNR array is reported in Fig. SI 1a (ESI†).

UV-visible spectroscopy

UV-visible absorption spectroscopy was used to measure the optical density of the colloidal dispersion of the AuNRs and for the optical characterization of the AuNR array. Measurements were performed using a Lambda 365 spectrophotometer from PerkinElmer. The measurements were carried out over a wavelength range of 400 to 1100 nm. To measure the OD600 of bacterial cell cultures, a diode array spectrophotometer HP8453 (Agilent Technologies) was used.

Scanning electron microscopy analysis

Scanning electron microscopy (SEM) micrographs were obtained using the high-resolution Scanning Electron Microscopy AURIGA from Zeiss at the Interdepartmental Research Center on Nanotechnologies Applied to Engineering (C.N.I.S.) of Sapienza University of Rome. Micrographs were acquired at magnifications of 100k× and 250k× to characterize the AuNRs array substrate. For the analysis performed after the biosensing experiments, micrographs were taken at a magnification of 50k×.

Preparation of AuNRs array for SEM characterization following the biosensing experiment. The SEM analysis of bioactive AuNR array immersed in the mixture of *E. coli* and *S. typhimurium*, after the biosensing experiment, was performed after a dehydration and fixing procedure. In particular, the sample was dehydrated by sequential immersion for 10 min in ethanol/water solutions at an increasing ethanol percentage: 10%, 20%, 30%, 40%, 50%, 60%, 70%, 80%, 90%, 95%, and 100%.

Subsequently, samples were fixed by immersion for 2 h in 2.5% glutaraldehyde in a PBS, pH 7.3 solution and left to dry overnight. Finally, a thin layer of Cr (5 nm) was sputtered before inserting the samples into the SEM vacuum chamber.

Measurements were performed at the Interdepartmental Research Center on Nanotechnologies Applied to Engineering (C.N.I.S.) of Sapienza University of Rome. The *ImageJ* software was utilized for performing the statistical analysis of the SEM micrographs.

Atomic force microscopy characterization

Atomic force microscopy (AFM) measurements were performed using the AFM Veeco Icon and the AFM Veeco Multimode at the Interdepartmental Research Center on Nanotechnologies Applied to Engineering (C.N.I.S.) of Sapienza University of Rome. The characterization was conducted on an area of 2 μm × 2 μm.

Realization of a bio-functionalization chamber

An *ad hoc* functionalization chamber was realized to bioactivate the AuNR arrays with two different monoclonal antibodies in two distinct areas of the array.

The chamber, as depicted in Fig. SI 2 (ESI†), was meticulously crafted. It involved sealing two glass slides (1.5 cm × 1.5 cm) on a glass support (2.5 cm × 2.5 cm), positioned perpendicular to the glass support plane and at a precise distance of 0.5 cm from each other. Two additional glass slides (1.0 cm × 1.5 cm) were then added, each in contact with the edge of the former glass slides, resulting in a glass chamber open at the top.

The sealing steps were performed using NOA 61 as a glue polymerized with a UV gun.

The chamber was sequentially rinsed with methanol and acetone and dried under a nitrogen stream before use.

Site-specific AuNR array functionalization with two monoclonal antibodies

The multiplex biosensing experiments were performed using AuNR arrays, measuring 1.5 cm × 1.5 cm. Each array was marked with a diamond tip by gently creating a vertical line on the back side of the array. This line starts from the center and extends to the bottom of the glass substrate, perpendicular to the substrate edge, thus dividing the AuNRs array into two distinct areas: a1 and a2, respectively.

A micropipette was utilized to introduce 200 μL of a water solution of AbE 0.01 mg mL^{-1} into the chamber. The a1 of the AuNR array was immersed and left to incubate for 2 h. It was rinsed with Milli-Q water and dried under nitrogen flow.

The chamber was rinsed again, with water, methanol and acetone, dried and filled with 200 μL of a water solution of AbS 0.01 mg mL^{-1}. At this stage, the a2 of the AuNRs array was bioactivated with the AbS by immersing the a2 side in the 200 μL AbS solution for 2 h. The entire functionalization process was conducted at room temperature under physiological pH conditions. The pH of the solution was monitored using pH indicator strips. The resulting double-functionalized AuNRs/AbE/AbS array was rinsed with Milli-Q water and dried under nitrogen flow, before characterization and biosensing experiments. The absorption spectroscopic characterization of the AuNRs/AbE/AbS arrays was performed by separately analyzing the a1 and the a2 functionalized area with the AbE and AbS, respectively.

The optical window of the sample holder has an area of 38 mm^2. The a1 or a2 area dimensions are 7.5 mm × 15 mm, corresponding to 112 mm^2. Therefore, when the AuNRs/AbE/AbS samples are correctly introduced in the absorption spectrophotometer sample holder, performing an absorption measurement only on the desired area selectively is possible (Fig. SI 3, ESI†).

Simultaneous pathogens identification experiments. Three 20 mL glass beakers were filled with 4 mL of three different physiological solutions containing *E. coli* (10^3 CFU per mL), *S. typhimurium* (10^3 CFU per mL), and a mixture of the two bacteria, respectively. In particular, the mixed solution contained both the *E. coli* (10^3 CFU per mL) and *S. typhimurium* (10^3 CFU per mL).

Three AuNRs/AbE/AbS arrays were immersed in the *E. coli* solution, the *S. typhimurium* solution, and the mixed solution for 30 min, respectively. Subsequently, after rinsing and drying steps, the absorption spectrum of the three arrays was measured by analyzing both the a1 and the a2.

Fabrication of a plasmonic cascade AuNR array

To exploit the thermoplasmonic properties of AuNR array for PT water disinfection two AuNR arrays were assembled in a cascade-like configuration.

First, a single AuNR cell was produced to investigate the PT behavior of an AuNR array. To this end, a few drops of NOA-61 polymer glue (containing monodispersed 10 μm glass microbead spacers) were placed on the four corners of the AuNR array. Then, the AuNR array was covered with a 1 cm × 1 cm glass slide. The resulting cell (scheme reported in Fig. SI 1b, ESI†) was sealed for 1 minute under UV light (375 nm, 3.5 mW cm^{-2}) exposure. The AuNR cell possesses a uniform gap of about 10 μm.

The plasmonic cascade AuNR array was fabricated by assembling two AuNR arrays to investigate the PT disinfection properties. In this process, the polymeric glue NOA-61 was carefully applied to the corners of one AuNR array, thus enabling the integration of the second AuNR array on the top. The latter was placed so that the two arrays were in direct contact, with a 10 μm gap. The resulting cascade AuNR array, illustrated in Fig. SI 1c (ESI†), was sealed through a 1 min exposure to UV light (375 nm, 3.5 mW cm^{-2}).

At this stage, two additional cover glass (CG) slides (1 cm × 1 cm) were integrated on top of the cascade AuNR array using the same procedure for realizing the cells, resulting in the AuNR array CG, depicted in Fig. SI 1d (ESI†).

PT characterization of AuNR arrays

For the PT characterization of the AuNR array, an 808 nm continuous near-infrared (NIR) laser (PowerLine from Coherent) was employed. The NIR laser beam has a rectangular profile, which was converted into an almost circular spot utilizing a 20 cm focal length elliptical lens. A power meter was used to accurately measure the power of the NIR laser. The temperature changes induced by the AuNR array's PT irradiation were quantified using a FLIR A655sc thermal imaging camera. The camera captures thermal images at a resolution of 640 × 480 pixels, possessing an accuracy of ±0.2 °C. Seamlessly integrated with FLIR ResearchIR Max software, it captures and processes the acquired thermal data, ensuring precision and reliability in the analysis. The PT characterization with the NIR laser was performed by varying the laser intensity from 1.193 W cm^{-2} to 8.530 W cm^{-2}. The thermal imaging camera software recorded a 5-minute and 5-second video for each measure. For the first 5 s of the acquisition time, the laser was blocked with a shutter, ensuring a stable baseline; then, the laser was left to impinge the sample for 3 min. The sample was left to cool down for 2 min, and finally, the thermal imaging recording was stopped. A deliberate interval was observed between successive measurements, facilitating the sample's return to ambient temperature.

PT optical setup for water disinfection

For PT water disinfection experiments, a CW fiber-coupled 808 nm laser source (MDL-H-808 from CNI Laser) was used. The laser intensity was tuneable up to a maximum of 2.32 W cm^{-2}. The optical setup was arranged so that the laser light irradiates, from the bottom, a 20 mL beaker filled with 1.1 mL of tap water containing the plasmonic cascade of AuNR array CG. Notably, the geometry of the optical setup was purposely designed to ensure uniform irradiation of the cascade AuNR array CG. The backer was then placed inside a polystyrene box (cubic shape, side 20 cm) to provide thermal insulation, thus minimizing the heating dissipation with the environment. The high-resolution thermal camera (see Section 2.7 for details) was used to record the temperature variation of the water bulk during the irradiation. The setup also includes a thermometer with a temperature probe PT56L (Thermo Scientific) to validate measurements obtained from the analysis of thermographic images. The thermometer has a diameter of 3 mm, a probe length of 200 mm, and an accuracy at 100 °C of ±0.16 °C. Data acquisition with the thermometer was performed using the RealTerm software.

Bacteria growth and counting

E. coli K12 MG1655 was used for the experiments (always performed in duplicate). For bacterial growth, a single colony from a freshly streaked plate was inoculated into 2 mL of minimal medium E supplemented with 0.4% glucose (EG medium), pH 7.0,[26] and bacteria were allowed to grow overnight under orbital shaking (150 rpm) at 37 °C. The following day, the OD600 of each overnight culture was registered by diluting 100 μL into 900 μL of sterile saline solution (0.9% w/v NaCl in water). The bacterial density was therefore calculated using the conversion factor OD600 1.0 = 5×10^8 colony forming units (CFU) per mL and by testing the exact value by plating appropriate dilutions of each overnight culture. A 10^6 CFU per mL stock was then prepared in physiological solution and used for biosensing or disinfection experiment.

S. typhimurium LT2 was growth in 2 mL of Luria Bertani (LB) medium at 37 °C under orbital shaking, overnight. After growth, bacterial cells were collected by centrifugation at 4300 rpm for 10 minutes. The spent supernatant was removed and the pellet was reconstituted in an equal saline solution. The concentration in CFU per mL was determined through serial dilution and plating on Luria Bertani (LB) plates, with subsequent growth at 37 °C, yielding a concentration of 1.17×10^9 CFU per mL.

For *E. coli* disinfection experiments, further dilutions, according to the experimental setup, *i.e.*, approx. 6×10^4 CFU per mL in tap water were used. During the irradiation time, an aliquot (100 μL, corresponding to the starting material of 6×10^3 CFU) was taken from the beaker at each time point. The bacteria that had survived the treatment were counted by plate counting following overnight recovery in LB agar plates at 37 °C. Only for the last point (*i.e.*, 60 min) was all the residual volume (on average 350 μL, corresponding to the starting material of 2.1×10^4 CFU) used for plating.

Numerical simulations

Finite element method (FEM) simulations were carried out to investigate the wavelength-dependent electromagnetic (EM) absorption spectrum of the AuNR array and estimate PT effects triggered by the NIR irradiation of AuNRs. Modeling of the structure under analysis, performed by COMSOL Multiphysics™, Sweden commercial software, was targeted to simulate the excitation of LSPR modes on the AuNR array and the numerical estimation of laser power absorption upon thermal relaxation of EM oscillations. Evaluating energy conversion at the nanoscale allows the validation of the theoretical modeling of heat transfer mechanisms and the assessment of the overall PT efficiency of the AuNR array.

Results and discussion

Optical, morphological and PT characterization of AuNR array

The biosensing performance of the proposed AuNR/AbE/AbS array strongly relies on the sensitivity of the longitudinal plasmon band (LPB) wavelength to *n* changes. To fully exploit the *n* sensitivity of AuNRs, as well as the PT properties a worthwhile approach is to reproduce on a solid support the optical feature of a AuNR colloidal dispersion.[18] In this perspective, we optimized a previously reported protocol based on the immersive layer-by-layer (or LbL) PE assembly technique.[18] We selected PAH and PSS as suitable PE because they efficiently promote the successful incorporation of AuNRs on a glass substrate, giving rise to a stable and uniform AuNR array.[18,28,29] The PEs were dissolved in NaCl 0.5 M, thus benefiting from the effect of the ionic strength. Indeed, Na^+ and Cl^- ions at molar concentrations higher than 0.2 M exert a charge shielding effect which reduces the accumulation of PE molecules with the same electrical charge (electrosteric repulsion),[30] promoting, instead, the electrostatic attraction of the PEs with opposite charge. Moreover, Na^+ and Cl^- ions create a bilayer between two PE layers with an opposite charge. These two effects significantly increase the electrostatic attraction between cationic and anionic PE and, consequently, strengthen their adhesion.[31]

The absorption spectrum of the resulting AuNR array is reported in Fig. 1a. It shows a transverse plasmon band centred at 513 nm and a LPB at 763 nm. The LPB has a full-width half maximum (FWHM) of 103 nm. Therefore, the plasmon bands are sharp and symmetrical and resemble the optical features of the respective AuNRs colloidal dispersion, shown in Fig. 1b. Moreover, as detailed in Section SI 4 of ESI,† the AuNRs' LPB position is sensitive to *n* variations.

These features suggest sample uniformity and the absence of AuNR aggregates. The topographic analysis obtained by AFM and reported in Fig. 1c also indicates a uniform AuNR distribution. It shows an even distribution of asperities with an anisotropic morphology compatible with AuNRs. The height profile in Fig. 1d highlights that most of the asperities exhibit a height between 5 and 15 nm. Such a dimensional range is fully compatible with the shorter dimension of AuNRs. Moreover, Fig. 1c and d highlight the presence of some asperities higher than 10 nm, suggesting that some AuNRs are vertically oriented on the PEM. However, it's noteworthy that most nanostructures exhibit heights below 10 nm, suggesting the partial embedding of AuNRs within the PEM. Such experimental evidence supports the role played by the PEM as "glue molecules" accommodating AuNRs and ensuring their firm incorporation.

The AuNR array morphology was analyzed by SEM and reported in Fig. 1e and f. It points out a uniform distribution of the AuNRs with a fill fraction equal to 18.33. The even AuNRs distribution and the absence of aggregates are pivotal factors contributing to the remarkable optical properties observed in Fig. 1a. The spherical objects are noticeable in Fig. 1f and can be safely associated with vertically oriented AuNRs, previously evidenced in the AFM characterization. The SEM micrographs (Fig. 1e and f) were analyzed in detail using the *ImageJ* software, allowing us to perform a comprehensive statistical analysis (see Section SI 5 of ESI,† for more information). The statistical analysis encompassed several parameters, including the AuNRs' length, the interparticle distance, and the AuNRs' orientation, with respect to the vertical and horizontal axes. The statistical analysis conducted on the length of the AuNRs revealed that the mean value AuNRs length is 51.5 nm ± 3 nm, in agreement with the datasheet provided by the seller. The statistical distribution can be considered still Gaussian, although a percentage probability of 16% (see Section SI 5 of ESI,† and Fig. SI 5a)

The average distance between AuNRs was determined by measuring the length of the shorter segment connecting one selected AuNR with the four nearest AuNRs. The statistical

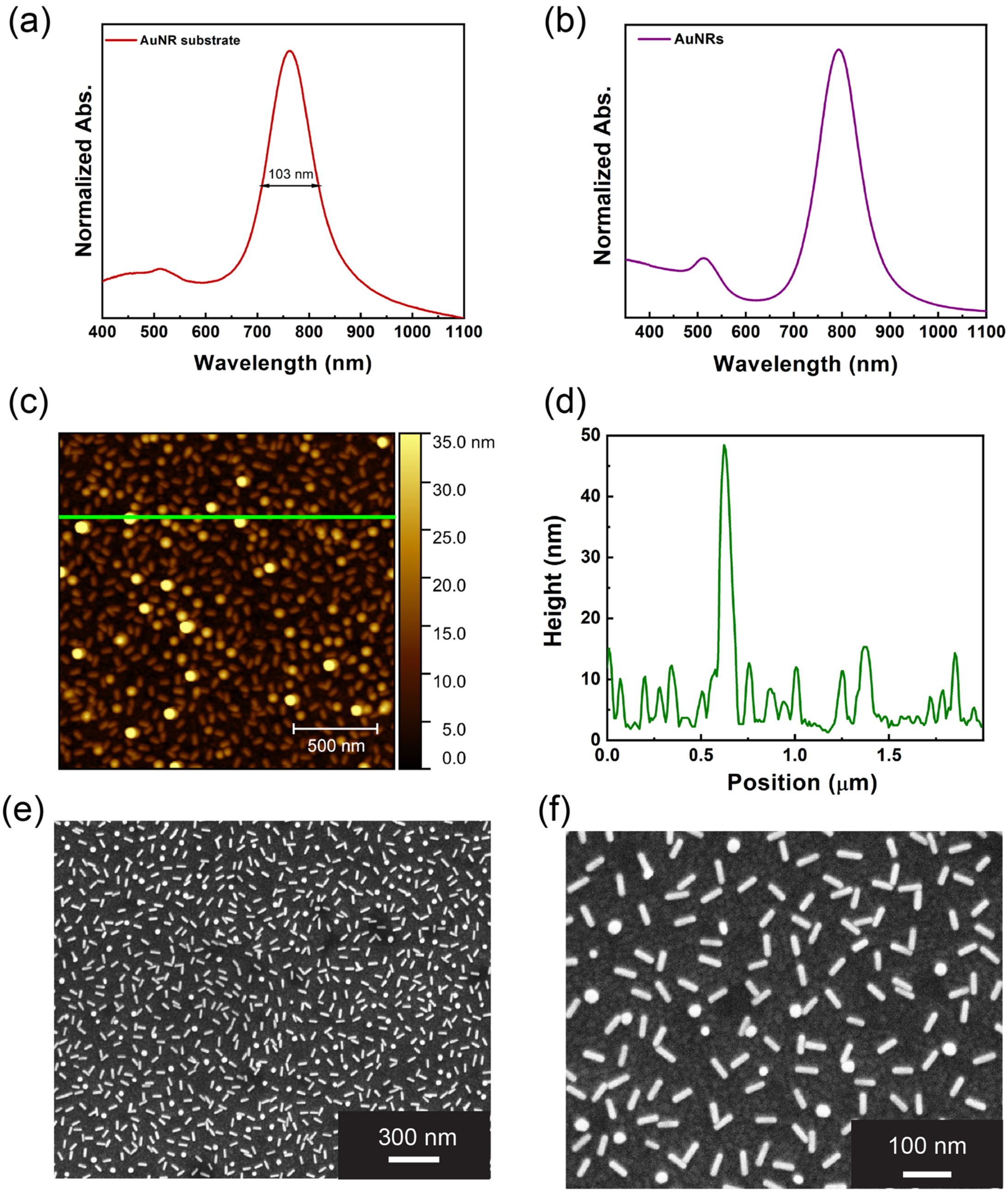

Fig. 1 Absorption spectrum of a representative AuNR array (a). Absorption spectrum of the AuNR colloidal dispersion (b). AFM image of the AuNR array (c) with the respective height profile (d) obtained along the green line presented in panel c. SEM micrograph of the AuNR array measured at 100k× magnifications (e) and 250k× magnifications (f).

analysis reveals that the interparticle distance values reported a normal distribution centred around the mean value of 75.4 ± 18.8 nm (see Section 5.2 of ESI,† and Fig. SI 5b).

To get insight into the AuNR's orientation, we considered the angle formed by AuNRs with respect to both the horizontal and vertical axes, giving rise to the horizontal and the vertical angles, respectively. The angles measured in our analysis ranged from 0° to 180°, with an average value of 84.9° and 80.3° for the horizontal and the vertical angle, respectively (Fig. SI 5c and d, ESI†). However, according to the chi-square test, the AuNRs orientation with respect to both the horizontal and the vertical axes can be considered statistically random, as detailed in Section SI 5.3 of the ESI.†

Simultaneous detection of *E. coli* and *S. typhimurium* by the logic-OR plasmonic biosensor

The AuNR array was utilized to realize a plasmonic biosensor whose optical behaviour mimics a logic-OR gate, sketched in Fig. 2a. The biosensor is designed to recognize *E. coli* and *S. typhimurium* cells dispersed in water either separately or simultaneously. To this end, the AuNRs array was functionalized using two monoclonal antibodies (Abs), the AbE and the

AbS, as biorecognition elements. The two Abs were incorporated in two distinct areas of the AuNRs array, namely a1 and a2 for the AbE and the AbS, respectively, as represented in Fig. 2b, resulting in the AuNRs/AbE/AbS plasmonic biosensor. The double Ab-functionalization was realized using the lab-made system schematized in Fig. SI 2 of ESI.†

Fig. 2c–h show the absorption spectra of three AuNRs arrays, analysed in the a1 area (c, e and g) and in the a2 area (d, f, and

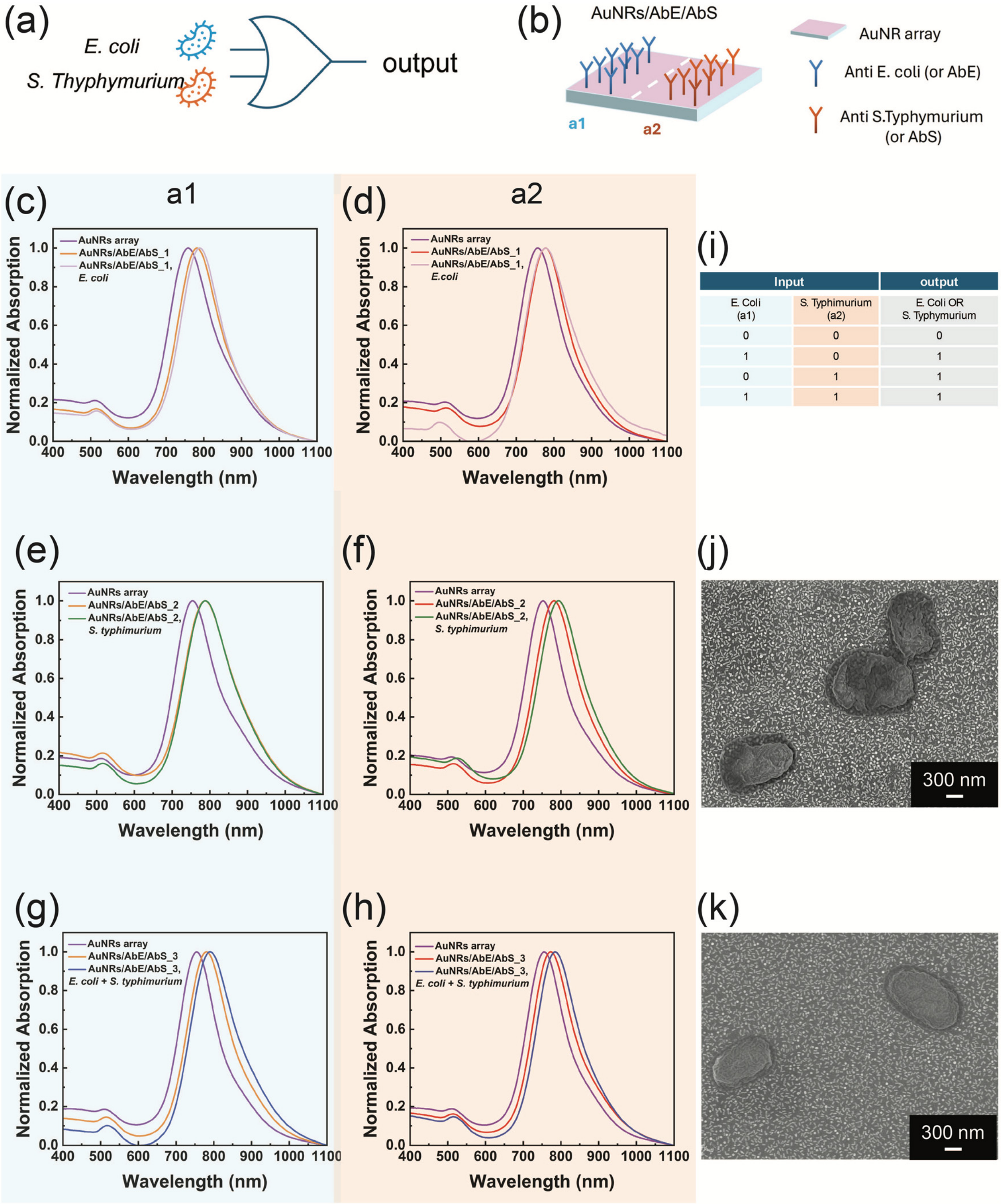

Input		output
E. Coli (a1)	S. Typhimurium (a2)	E. Coli OR S. Typhymurium
0	0	0
1	0	1
0	1	1
1	1	1

Fig. 2 Symbol of an OR gate presented according to the American National Standards Institute convention (a). Scheme of the AuNRs/AbE/AbS array realized to recognize *E. coli* in a1 s and *S. typhimurium* in a2, selectively (b). Normalized absorption spectrum of the a1 area (c) and a2 area (d) of an AuNRs/AbE/AbS array immersed in a 10^3 CFU per mL *E. coli* solution. Normalized absorption spectrum of the a1 area (e) and a2 area (f) of an AuNRs/AbE/AbS array immersed in a 10^3 CFU per mL *S. typhymurium* solution. Normalized absorption spectrum of the a1 area (g) and a2 area (i) of an AuNRs/AbE/AbS array immersed in a solution of *E. coli* (10^3 CFU per mL) and *S. typhymurium* (10^3 CFU per mL). All the plots of panels c–i show the absorption spectrum of the AuNR array, AuNRs/AbE/AbS array, and AuNRs/AbE/AbS array after the immersion in the specified bacteria solution. Table reporting the truth table of an OR gate (i). SEM micrographs of the a1 area (j) and a2 area (k) of the AuNRs/AbE/AbS_3 array after immersion in in a solution of *E. coli* (10^3 CFU per mL) and *S. typhymurium* (10^3 CFU per mL) evidencing the presence of *E. coli* cells and *S. typhimurium* cells, respectively on the AuNRs/AbE/AbS array. The micrographs were acquired at a magnification of 50k×.

h), identified as purple curved. The bioactivation resulted in three identical AuNRs/AbE/AbS plasmonic biosensors (AuNRs/AbE/AbS_1, AuNRs/AbE/AbS_2 and AuNRs/AbE/AbS_3). They were independently characterized in the a1 and the a2 area to assess the successful Ab incorporation.

The Ab functionalization produced a red-shift of the LPB both in the a1 and in the a2. In particular the AbE incorporation determined an average LPB red shift ($\Delta\lambda$) of 27 nm, (see orange curves in Fig. 2c, e and g) while the introduction of the AbS caused an average $\Delta\lambda$ of 23 nm as evidenced by the red curves in (Fig. 2d, f and h).

At this stage, the AuNRs/AbE/AbS_1 sample was immersed in a physiological solution of *E. coli* at 10^3 CFU per mL, rinsed, dried, and then analyzed using absorption spectroscopy.

This resulted in a $\Delta\lambda$ of 7 nm in the a1 (shown by the pink curve in Fig. 2c), while the LPB remained unchanged in the a2 (Fig. 2d). When the AuNRs/AbE/AbS_2 biosensor was immersed in a 10^3 CFU per mL solution of *S. typhimurium*, a negligible $\Delta\lambda$ (1 nm) was observed in the a1, while a shift of 12 nm occurred in the a2 (as indicated by the green curves in Fig. 2e and f). Finally, the AuNRs/AbE/AbS_3 sample was introduced into a mixture containing both *E. coli* and *S. typhimurium*, each at 10^3 CFU per mL. This resulted in a $\Delta\lambda$ of 10 nm in the a1 and 11 nm in the a2, as shown by the blue curves in Fig. 2g and h, respectively. The experimental data in Fig. 2c–h demonstrate that the a1 peak of the AuNRs/AbE/AbS specifically detects *E. coli*, while the a2 peak specifically detects *S. typhimurium*, in accordance with the biosensor's functionalization. Notably, the AuNRs/AbE/AbS plasmonic biosensor has proven capable of independently and simultaneously detecting *E. coli* and *S. typhimurium* when both bacteria are present in the analyte solution.

The optical response of the AuNRs/AbE/AbS arrays closely mimics the behaviour of a logic OR-gate, as shown in the table in Fig. 2i. The bioactive plasmonic nanoplatform generates a positive output (1) when one or both target bacteria are detected, corresponding to the logic states: 10, 01, or 11. In contrast, it produces a negative output (0) when neither bacterium is present, corresponding to the 00 logic state. This binary response accurately reflects the function of an OR-gate, where the output is true if at least one of the inputs is true. Thus, the system effectively translates biological detection into a digital logic function, highlighting its potential for advanced biosensing applications. Moreover, the AuNRs/AbE/AbS can produce distinct output (10 and 01), effectively excluding cross-reactivity between *E. coli* and *S. typhimurium*. Additionally, selective detection is ensured using monoclonal antibodies for strong specificity. The SEM micrographs in Fig. 2j and k emphasize the role of the AuNRs array bioactivation.

The SEM analysis of the a1 and a2 areas of the AuNRs/AbE/AbS_3 sample, performed after the biosensing experiment, evidences that *E. coli* cells and *S. typhimurium* cells are captured in two distinct areas of the AuNRs/AbE/AbS_3. Here, the antibodies trap the bacteria on the AuNRs/AbE/AbS arrays and at simultaneously initiate the specific antigen–antibody binding, leading to a specific optical response.

Photothermal characterization of AuNR array

To investigate the multifunctionality of the logic-OR gate plasmonic biosensor for PT pathogen disinfection, a detailed thermoplasmonic study was performed and reported in Section SI 6 of ESI.† Experimental data highlight the increase in $T_{\max}$ values as the laser intensity increases, reaching a $\Delta T_{\max}$ of 54.7 °C when the intensity was set at 8.53 W cm^{-2}.

Our experimental study was robustly supported by comprehensive numerical simulations, as meticulously detailed in Section SI 7 of ESI.† From an optical perspective, the numerical results (see Sections SI 7 and SI 8 of ESI†) pertaining to the absorption spectrum of the AuNR array not only confirmed the experimental findings but also provided additional insights. These insights included the relationship between the FWHM (Fig. SI 8a, ESI†), the distribution of the AuNRs' length deviation, and the effect of the partial submersion of AuNRs in the PEM, as experimentally evidenced by the AFM characterization (Fig. 1c). Furthermore, Fig. SI 8b (ESI†) demonstrates the thoroughness of our research process, as it shows a satisfactory agreement between the theoretical curves and the experimental results for each NIR laser intensity value. This level of agreement instils confidence in the reliability of our findings.

Leveraging the results obtained by PT characterization and numerical simulation, we investigate the proposed device as a high-performance thermo-optical transducer for bulk water disinfection.

To this end, two AuNR arrays were used to fabricate a cascade-like system, namely AuNR array CG, whose optical

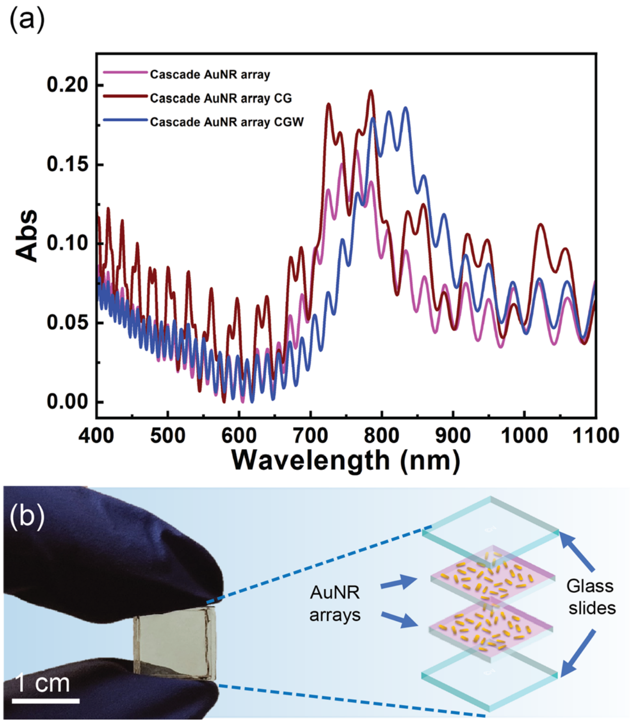

Fig. 3 Absorption spectra of the cascade AuNR array, cascade AuNR array CG, and cascade AuNR array infiltrated with water (cascade AuNR array CGW) (a). Digital picture of the cascade AuNR array CG (left) and schematic representation of the cascade AuNR array CG (right) (b).

properties are reported in Fig. 3a and sketched in Fig. 3b and Fig. SI 1d (ESI†). This cascade-like system was purposely chosen to amplify the PT properties of the single AuNR array, thus achieving a PT device that can generate a temperature increase that is fully suitable for performing PT water disinfection.

The absorption spectrum of the cascade AuNRs (Fig. SI 1c, ESI†), shown in the magenta line of Fig. 3a, displayed the LPB at 763 nm, at the same wavelength as the AuNR array (Fig. 1a). Moreover, interference fringes appeared in the spectra due to light interference in the gap between the two AuNR arrays incorporated one on top of the other. Upon modification to create the cascade AuNR array CG (illustrated in Fig. 3b and Fig. SI 1d, ESI†), the LPB position remains unchanged, as evidenced by the dark red line in Fig. 3a. However, upon infiltration with water (n = 1.33), a $\Delta\lambda$ of the LPB to 810 nm is observed, as depicted by the blue line in Fig. 3a. Fig. 3a shows that interference fringe patterns changed as additional gaps were introduced from the cascade AuNR array to the cascade AuNR array GC (Fig. 3a, dark red line). However, the position of the longitudinal peak remains unchanged. Consequently, the observed red-shift is primarily due to the LPB effect caused by water infiltration and not to interference fringes, which are simply an optical artifact from the cell's physical configuration. This shift aligns the LPB resonance with the emission wavelength of the NIR laser source (λ = 808 nm) employed in our study. Consequently, the PT behaviour of the plasmonic AuNR array CG was characterized to assess the suitability of this system as a thermo-optical transducer for water disinfection experiments.

Photothermal characterization of plasmonic cascade AuNR arrays and photothermal disinfection experiments

The PT response of the cascade AuNR array and the cascade AuNR array CG was investigated using the thermo-optical setup (Fig. SI 11a, ESI†) realized for PT disinfection experiments.

This meticulous PT study was carried out and reported in Section SI 9 of the ESI.† We focused our analysis on the average temperature values measured in tap water, as they are the values experienced by bacteria cells during PT water disinfection.

Experimental data evidenced the suitability of the AuNR array CG as a thermo-optical transducer for disinfection of bulk water, based on two effects.

The first is the role played by the n of the surrounding medium, as the immersion of the cascade AuNR array CG in water, shifted the LPB at a wavelength in resonance with the NIR laser emission wavelength, thus maximizing the PT heating.

The second is the effect of the thermal conductivity of the water.

Indeed, the higher average temperature values obtained in water (35.9 °C) than in a dry state (27.6 °C) (see Fig. SI 11b and c, ESI†) are imputable to the thermal conductivity of water (0.5918 W m^{-1} K^{-1} at 20 °C) that is higher to the thermal conductivity of air (0.025 W m^{-1} K^{-1} at 20 °C).

By replacing the thermal camera with a digital contact thermometer (Fig. SI 12a of ESI†), we obtained more accurate bulk temperature values, validating the experimental data obtained with the thermal camera.

Indeed, at the end of irradiation, the digital contact thermometer measured an average temperature value of 38.8 °C. This value is consistent with the data obtained from the analysis of thermographic images (Fig. SI 11c, blue line, ESI†) but also evidence of a uniform heat distribution throughout the volume of water in 30 minutes of illumination.

The optical set-up and the experimental procedure for PT water disinfection were further improved by introducing an isolating container and extending the irradiation time to 50 min.

This improvement led to a temperature increase to 59.1 °C (Fig. SI 12c, blue line, ESI†). As this value is known to induce bacteria inactivation,[17,18] these experimental conditions were used for performing PT disinfection experiments after further validation.

While based on the same platform, the devices used for photothermal disinfection and biosensing are distinct. Specifically, the biosensor is biofunctionalized, whereas the cascade AuNR platform employed for photothermal disinfection is not. This distinction underscores the versatility of the platform while mitigating concerns about cross-effects. Moreover, the maximum temperature achieved during photothermal disinfection experiments remains below the 80–90 °C threshold required for antibody denaturation.[23] These factors confirm that the photothermal properties utilized for disinfection do not compromise the biosensing functionality of the platform.

An additional PT experiment was carried out using the thermal camera and the digital immersion thermometer to measure the time-temperature profile. The setup in Fig. SI 12a (ESI†) was utilized. During 60 min of NIR laser irradiation, the isolating box was opened at regular intervals (for 3 s) to capture the thermographic images.

The experimental data reported in Fig. 4a (cyan dots) are consistent with the bulk temperature values obtained from the thermometer and shown in the red line of Fig. 4a. This data set demonstrates that the system's eventual and momentary perturbation did not significantly alter the heating process.

The experimental data unequivocally state the capability of the plasmonic cascade AuNR array CG to achieve PT disinfection of tap water through PT heating. Hence, the configuration outlined in Fig. SI 12a (ESI†) was employed to conduct PT disinfection experiments utilizing the cascade AuNR array CG for PT heating. In these experiments, a glass beaker was filled with 1.1 mL of tap water deliberately contaminated with *E. coli* cells (selected as the model pathogen), yielding a bacterial concentration of 6 × 10^4 CFU per mL. At scheduled time intervals, the lid of the insulating container was shortly opened to allow the withdrawal of 100 μL of contaminated tap water from the beaker. Subsequently, the aliquot was transferred into a sterile Eppendorf tube and, where necessary (*i.e.*, time 0, 10, and 20 min), dilutions in physiological solution were made before plating out so to have a number of bacteria on the LB agar plate appropriate for counting. The results reported in Fig. 4e evidence a progressive decrease in the *E. coli* concentration (viability) during the irradiation time. In particular, after 30 minutes of irradiation, no viable cells were detected resulting in a *E. coli* concentration decrease by more than four orders of magnitude.

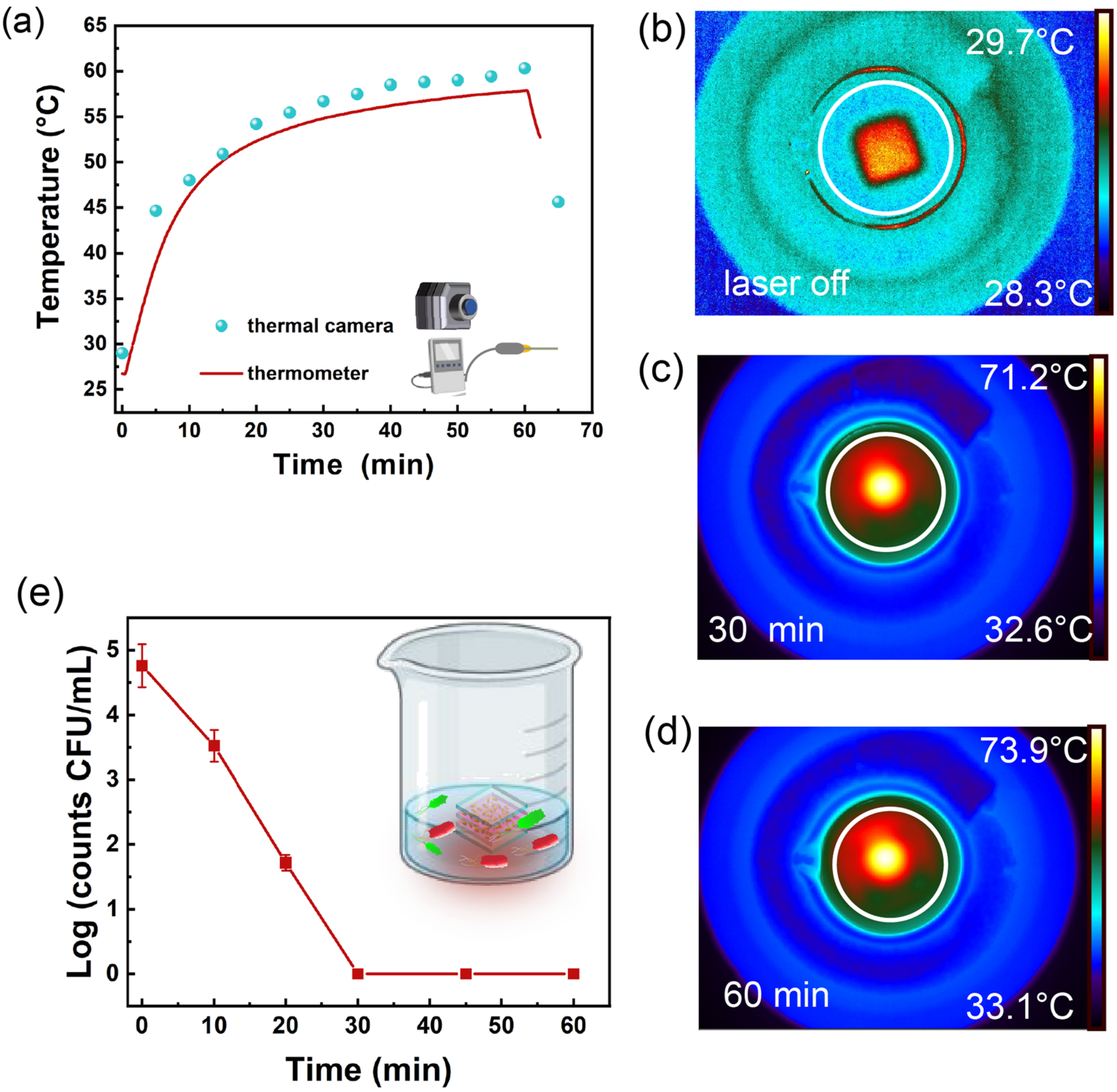

Fig. 4 Temperature value as a function of irradiation time, recorded *via* a digital contact thermometer (red line) and thermal camera (cyan dots) (a) thermographic images of the beaker filled with 1.1 mL of tap water obtained before irradiation (b), after 30 min of irradiation (c) and at 60 min of irradiation (d). The white circle in (b), (c) and (d) indicates the ROI. Viability of *E. coli* cells as a function of irradiation time during the PT disinfection experiment; the mean value is reported as calculated CFU mL^{-1} with the corresponding standard error of the mean (e). In the inset of (e), a schematic of the beaker containing contaminated water and the AuNR array CG sample. is reported.

Conclusions

This work presents the development, characterization, and validation of a multifunctional AuNR array fabricated using the LbL assembly method. The array's optical, morphological, and PT properties are experimentally investigated and validated by numerical simulations. The AuNR array is functionalized with monoclonal antibodies specific to *E. coli* and *S. typhimurium* to enable multipathogen detection. The AuNR array mimics the behaviour of a logic OR-gate, where the LPB red-shifts when one or both bacteria are present. At the same time, no shift occurs in bacteria-free water. This selective detection, confirmed *via* absorption spectroscopy and SEM microscopy, allows simultaneous identification of the pathogens in water using simple spectroscopy. A cascade AuNR array shows a shift in the LPB from 750 nm to 808 nm upon water infiltration, aligning with NIR laser emissions for effective PT disinfection. The array raised the water temperature to 59.1 °C in 50 minutes, leading to the complete disinfection of *E. coli*-contaminated water in 30 minutes, reducing the *E. coli* viability by about five orders of magnitudes. The AuNR array remains reusable and has stable optical properties over several months. These findings highlight the potential for cost-effective water monitoring and purification technologies, particularly in regions with water scarcity. The proposed system can be easily integrated with a microfluidic chamber in the future to enable the multiple and simultaneous detection of pathogens and chemical compounds relevant to water safety. Ongoing research aims to optimize PT performance under solar light, scale up treated volumes, improve biosensing sensitivity, and perform multiple pathogens detection.

Author contributions

The manuscript was written through contributions of all authors. All authors have given approval to the final version of the manuscript.

Data availability

We confirm that no databases were used and no references to such databases are contained in the manuscript or ESI.† We are happy to share the raw data upon reasonable request to the corresponding authors.

Conflicts of interest

There are no conflicts to declare.

Acknowledgements

This work has been supported by the "NATO – Science for Peace and Security Programme (SPS-G7425, CLC-BIODETECT)", by the Air Force Office of Scientific Research, Air Force Material Command, U.S. Air Force. "Digital optical network encryption with liquid-crystal grating metasurface perfect absorbers" FA8655-22-1-7007 (P. I., L. De Sio, EOARD 2022-2025), and by EU funding within the NextGenerationEU-MUR PNRR Extended Partnership initiative on Emerging Infectious Diseases (Project no. PE00000007, INF-ACT).

References

1 Centers for Disease Control and Prevention (CDC). Causes of Water Contamination. Available online: **https://www.cdc.gov/drinking-water/causes**.

2 H. Sohrabi, A. Hemmati, M. R. Majidi, S. Eyvazi, A. L. Jahanban-Esfahlan, B. Baradaran, R. Adlpour-Azar, A. Mokhtarzadeh and M. L. de la Guardia, Recent advances on portable sensing and biosensing assays applied for detection of main chemical and biological pollutant agents in water samples: a critical review, *TrAC, Trends Anal. Chem.*, 2021, **143**, 116344.

3 V. Naresh and N. Lee, A review on biosensors and recent development of nanostructured materials-enabled biosensors, *Sensors*, 2021, **21**, 1109.

4 B. E. Cowie, V. Porley and N. Robertson, Solar Disinfection (SODIS) Provides a Much Underexploited Opportunity for Researchers in Photocatalytic Water Treatment (PWT), *ACS Catal.*, 2020, **10**, 11779–11782.

5 K. G. McGuigan, R. M. Conroy, H.-J. Mosler, M. du Preez, E. Ubomba-Jaswa and P. Fernandez-Ibañez, Solar water disinfection (SODIS): a review from bench-top to roof-top, *J. Hazard. Mater.*, 2012, **235**, 29–46.

6 Z. Tang, D. Ma, Q. Chen, Y. Wang, M. Sun, Q. Lian, J. Shang, P. K. Wong, C. He, D. Xia and T. Wang, Nanomaterial-enabled photothermal-based solar water disinfection processes: fundamentals, recent advances, and mechanisms, *J. Hazard. Mater.*, 2022, **437**, 129373.

7 D. S. Lantagne and T. F. Clasen, Use of Household Water Treatment and Safe Storage Methods in Acute Emergency Response: Case Study Results from Nepal, Indonesia, Kenya, and Haiti, *Environ. Sci. Technol.*, 2012, **46**, 11352–11360.

8 L. Wang, Y. Feng, K. Wang and G. Liu, Solar water sterilization enabled by photothermal nanomaterials, *Nano Energy*, 2021, **87**, 106158.

9 H. Miao, Z. Teng, S. Wang, L. Xu, C. Wang and H. Chong, Recent advances in the disinfection of water using nanoscale antimicrobial materials, *Adv. Mater. Technol.*, 2019, **4**, 1800213.

10 S. Roy, J. Roy and B. Guo, Nanomaterials as multimodal photothermal agents (PTAs) against 'Superbugs', *J. Mater. Chem. B*, 2023, **11**, 2287–2306.

11 Y. Yang, H. P. Feng, C. G. Niu, D.-W. Huan, H. Guo, C. Liang, H. Y. Liu, S. Chen and N. Tang, Constructing a plasma-based Schottky heterojunction for near-infrared-driven photothermal synergistic water disinfection: synergetic effects and antibacterial mechanisms, *Chem. Eng. J.*, 2021, **426**, 131902.

12 X. Cui, Q. Ruan, X. Zhuo, X. Xia, J. Hu, R. Fu, Y. Li, J. Wang and H. Xu, Photothermal nanomaterials: a powerful light-to-heat converter, *Chem. Rev.*, 2023, **123**, 6891–6952.

13 S. Eustis and M. A. El-Sayed, Why gold nanoparticles are more precious than pretty gold: noble metal surface plasmon resonance and its enhancement of the radiative and nonradiative properties of nanocrystals of different shapes, *Chem. Soc. Rev.*, 2006, **35**, 209–217.

14 L. Wang, M. Hasanzadeh Kafshgari and M. Meunier, Optical properties and applications of plasmonic-metal nanoparticles, *Adv. Funct. Mater.*, 2020, **30**, 2005400.

15 S. Loeb, C. Li and J. H. Kim, Solar Photothermal Disinfection using Broadband-Light Absorbing Gold Nanoparticles and Carbon Black, *Environ. Sci. Technol.*, 2018, **52**, 205–213.

16 D. Stoia, L. De Sio, F. Petronella and M. Focsan, Recent advances towards point-of-care devices for fungal detection: emphasizing the role of plasmonic nanomaterials in current and future technologies, *Biosens. Bioelectron.*, 2024, **255**, 116243.

17 F. Petronella, T. Madeleine, V. De Mei, F. Zaccagnini, M. Striccoli, G. D'Alessandro, M. Rumi, J. Slagle, M. Kaczmarek and L. De Sio, Thermoplasmonic Controlled Optical Absorber Based on a Liquid Crystal Metasurface, *ACS Appl. Mater. Interfaces*, 2023, **15**, 49468–49477.

18 M. L. Sforza, F. Petronella, D. De Biase, F. Zaccagnini, S. In Lim, U. A. Butt, A. d'Alessandro, N. P. Godman, D. R. Evans, M. McConney, K. Jeong and L. De Sio, Cascade Structured Plasmonic Liquid Crystal Biosensor for the Rapid Detection of Harmful Bacteria Dispersed in Potable Water, *Adv. Sensor Res.*, 2024, **3**, 2300201.

19 F. Zaccagnini, D. De Biase, F. Bovieri, G. Perotto, E. Quagliarini, I. Bavasso, G. Mangino, M. Iuliano, A. Calogero, G. Romeo, D. P. Singh, F. Pierini, G. Caracciolo, F. Petronella and L. De Sio, Multifunctional FFP2 Face Mask for White Light Disinfection

and Pathogens Detection using Hybrid Nanostructures and Optical Metasurfaces, *Small*, 2024, **20**, 2400531.

20 G. M. Akselrod, J. Huang, T. B. Hoang, P. T. Bowen, L. Su, D. R. Smith and M. H. Mikkelsen, Large-Area Metasurface Perfect Absorbers from Visible to Near-Infrared, *Adv. Mater.*, 2015, **15**(27), 8028–8034.

21 F. Zaccagnini, P. Radomski, M. L. Sforza, P. Ziółkowski, S.-I. Lim, K.-U. Jeong, D. Mikielewicz, N. P. Godman, D. R. Evans, J. E. Slagle, M. E. McConney, D. De Biase, F. Petronella and L. De Sio, White light thermoplasmonic activated gold nanorod arrays enable the photo-thermal disinfection of medical tools from bacterial contamination, *J. Mater. Chem. B*, 2023, **11**, 6823–6836.

22 S. Y. Oh, N. S. Heo and S. Shukla, *et al.*, Development of gold nanoparticle-aptamer-based LSPR sensing chips for the rapid detection of Salmonella typhimurium in pork meat, *Sci. Rep.*, 2017, **7**, 10130.

23 F. Petronella, D. De Biase, F. Zaccagnini, V. Verrina, S.-I. Lim, K.-U. Jeong, S. Miglietta, V. Petrozza, V. Scognamiglio, N. P. Godman, D. R. Evans, M. McConney and L. De Sio, Label-free and reusable antibody-functionalized gold nanorod arrays for the rapid detection of *Escherichia coli* cells in a water dispersion, *Environ. Sci.: Nano*, 2022, **9**, 3343–3360.

24 A. Ghazy, R. Nyarku, R. Faraj, K. Bentum, Y. Woube, M. Williams, E. Alocilja and W. Abebe, Gold nanoparticle-based plasmonic detection of Escherichia coli, *Salmonella enterica*, *Campylobacter jejuni*, and *Listeria monocytogenes* from bovine fecal samples, *Microorganisms*, 2024, **12**, 1069.

25 Y. Zhao, Z. Zhang, Y. Ning, P. Miao, Z. Li and H. Wang, Simultaneous quantitative analysis of *Escherichia coli*, *Staphylococcus aureus* and *Salmonella typhimurium* using surface-enhanced Raman spectroscopy coupled with partial least squares regression and artificial neural networks, *Spectrochim. Acta, Part A*, 2023, **293**, 122510.

26 M. A. Khomutov, F. Giovannercole, L. Onillon, M. V. Demiankova, B. F. Vasilieva, A. I. Salikhov, S. N. Kochetkov, O. V. Efremenkova, A. R. Khomutov and D. De Biase, A Desmethylphosphinothricin Dipeptide Derivative Effectively Inhibits *Escherichia coli* and *Bacillus subtilis* Growth, *Biomolecules*, 2023, **13**, 1451.

27 D. De Biase, A. Tramonti, F. Bossa and P. Visca, The response to stationary-phase stress conditions in *Escherichia coli*: role and regulation of the glutamic acid decarboxylase system, *Mol. Microbiol.*, 1999, **32**(6), 1198–1211.

28 E. Guzmán, R. G. Rubio and F. Ortega, A closer physico-chemical look to the Layer-by-Layer electrostatic self-assembly of polyelectrolyte multilayers, *Adv. Colloid Interface Sci.*, 2020, **282**, 102197.

29 E. Guzmán, H. A. Ritacco, F. Ortega and R. G. Rubio, Growth of Polyelectrolyte Layers Formed by Poly(4-styrenesulfonate sodium salt) and Two Different Polycations: New Insights from Study of Adsorption Kinetics, *J. Phys. Chem. C*, 2012, **116**, 15474–15483.

30 E. Blomberg, E. Poptoshev and F. Caruso, Surface interactions during polyelectrolyte multilayer build-up. 2. The effect of ionic strength on the structure of preformed multilayers, *Langmuir*, 2006, **22**, 4153–4157.

31 A. McAloney, M. Sinyor, V. Dudnik and M. C. Goh, Atomic force microscopy studies of salt effects on polyelectrolyte multilayer film morphology, *Langmuir*, 2001, **17**, 6655–6663.